Supplement of Atmos. Chem. Phys., 21, 14275–14291, 2021
https://doi.org/10.5194/acp-21-14275-2021-supplement

Atmospheric Chemistry and Physics
Open Access
EGU

Supplement of

The driving factors of new particle formation and growth in the polluted boundary layer

Mao Xiao et al.

Correspondence to: Urs Baltensperger (urs.baltensperger@psi.ch) and Imad El Haddad (imad.el-haddad@psi.ch)

Radical chemistry in CLOUD chamber

HO_2 is produced by the OH reactions with O_3 and VOCs in the experiments. The latter pathway dominates the HO_2 production rates, but also the RO_2 production rates (which means that in the absence of NO the RO_2-HO_2 ratios are fairly constant). The major sinks of HO_2 are self-reaction and reaction with NO. HO_2 concentrations are a few 10^9 cm^{-3} based on calculations. The ratio of N containing HOMs to total HOMs reaches 50 % of its maximum at 60-120 ppt NO. Given $k_{RO2+NO} = 10^{-11}$ $molecule^{-1}$ cm^3 s^{-1}, and $k_{RO2+HO2} = 2.5 \times 10^{-11}$ $molecule^{-1}$ cm^3 s^{-1}, the HO_2 concentration is estimated to be around 5×10^8 - 1×10^9 molecules cm^{-3} for aromatic oxidation experiments.

In the absence of NO (i.e., extremely low NO_x), HO_2 is expected to determine the lifetime of RO_2 because the HO_2+RO_2 channel is faster than the RO_2+RO_2 channel for most RO_2 radicals. There can be an exception for the highly oxygenated RO_2 radicals, which can self-terminate forming dimers (Berndt et al., 2018). In the ambient atmosphere, under low-NO_X conditions, OH reacts with CO and small oxygenated hydrocarbons to HO_2 radicals directly without first producing high molecular-weight RO_2 radicals, which increases the importance of the HO_2+RO_2 channel compared to CLOUD, decreasing dimer formation (Schervish and Donahue, 2020). Therefore, dimer formation rates from aromatics and hence new-particle formation rates under low-NO_X conditions in CLOUD should be considered as upper bounds.

At the range of precursor concentrations studied here, a few hundred ppt of NO is sufficient to dominate the sink of both HO_2 and RO_2, confirmed by checking the ratio of N-containing HOMs to total HOMs vs NO concentration. The addition of NO decreases both RO_2 and HO_2 but HO_2 would be recycled partially via RO_2+NO -> alkoxy radicals, which signifies that RO_2 self-termination is not at all favored compared to RO_2+NO and RO_2+HO_2. Therefore, under both low- and high-NO_X conditions, the dimer formation branching ratios would not be higher than simulated at CLOUD.

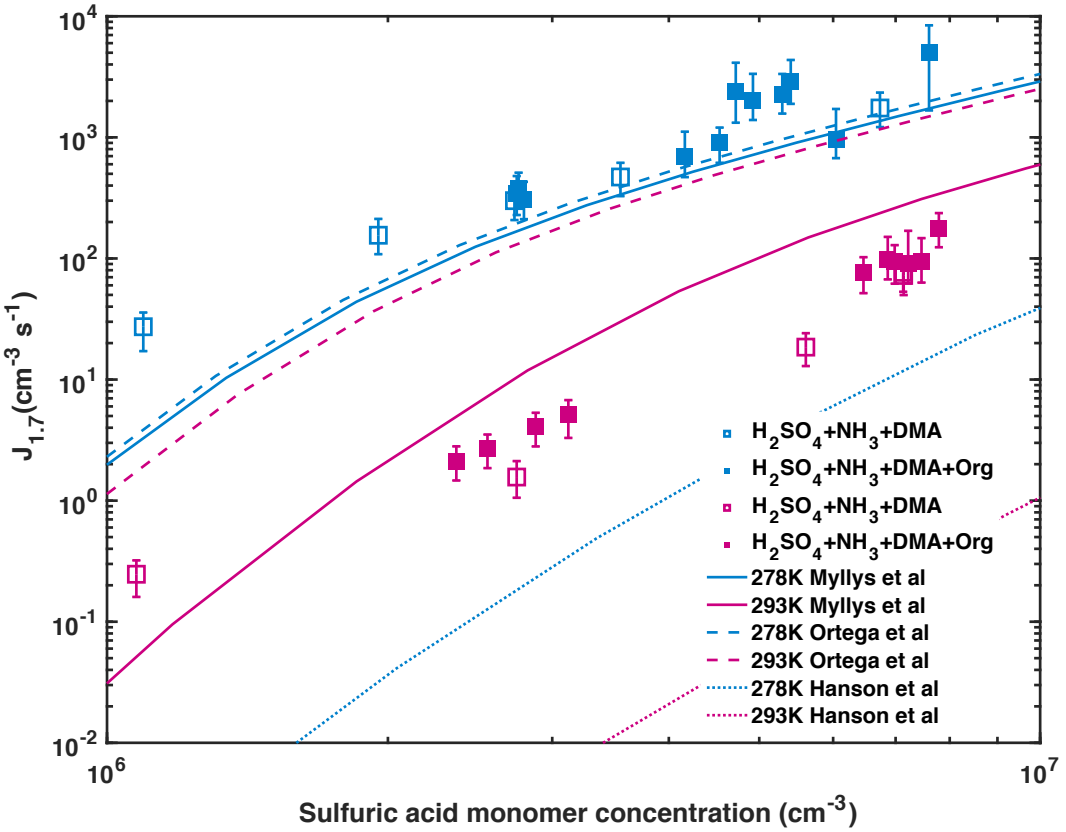

Figure S1: Modelled particle formation rates at 1.7 nm diameter from sulfuric acid with NH_3 and DMA compared with our measurements at 293 and 278 K. Experiments were performed at 278 K (cyan) or 293 K (magenta) with 1 to 2 ppbv NH_3 and 4 pptv DMA. Filled and open symbols indicate presence or absence of organics, respectively. The error bars refer to the measurement uncertainties for the particle formation rates. Solid and dashed lines are calculated with the kinetic model by implementing sulfuric acid - DMA cluster evaporation rates based on thermodynamic data from Myllys et al. (2019) (solid line), Ortega et al. (2012) (dashed line) and from Hanson et al. (2017) (dotted line), respectively. Modelled results based on binding energies for H_2SO_4-DMA clusters from Myllys et al (2019). follow the same trends as our measurements while other published binding energies for H_2SO_4--DMA clusters fail to reproduce the temperature dependency of the measured $J_{1.7}$. The tightly bound clusters theoretically predicted by Ortega et al. (2012) result in minor evaporation, leading to formation rates close to kinetic limits even at high temperatures. Note that the quantum chemical method used tends to overestimate binding energy values (Leverentz et al., 2013), and a reduction of the values at 298 K for the H_2SO_4-DMA cluster (-15.4 to -11 kcal mol^{-1}) and for $(H_2SO_4)_2$-DMA (-19.48 to -18 kcal mol^{-1}), as suggested by Hanson et al. (2017), results in considerably lower $J_{1.7}$ values compared to our observations.

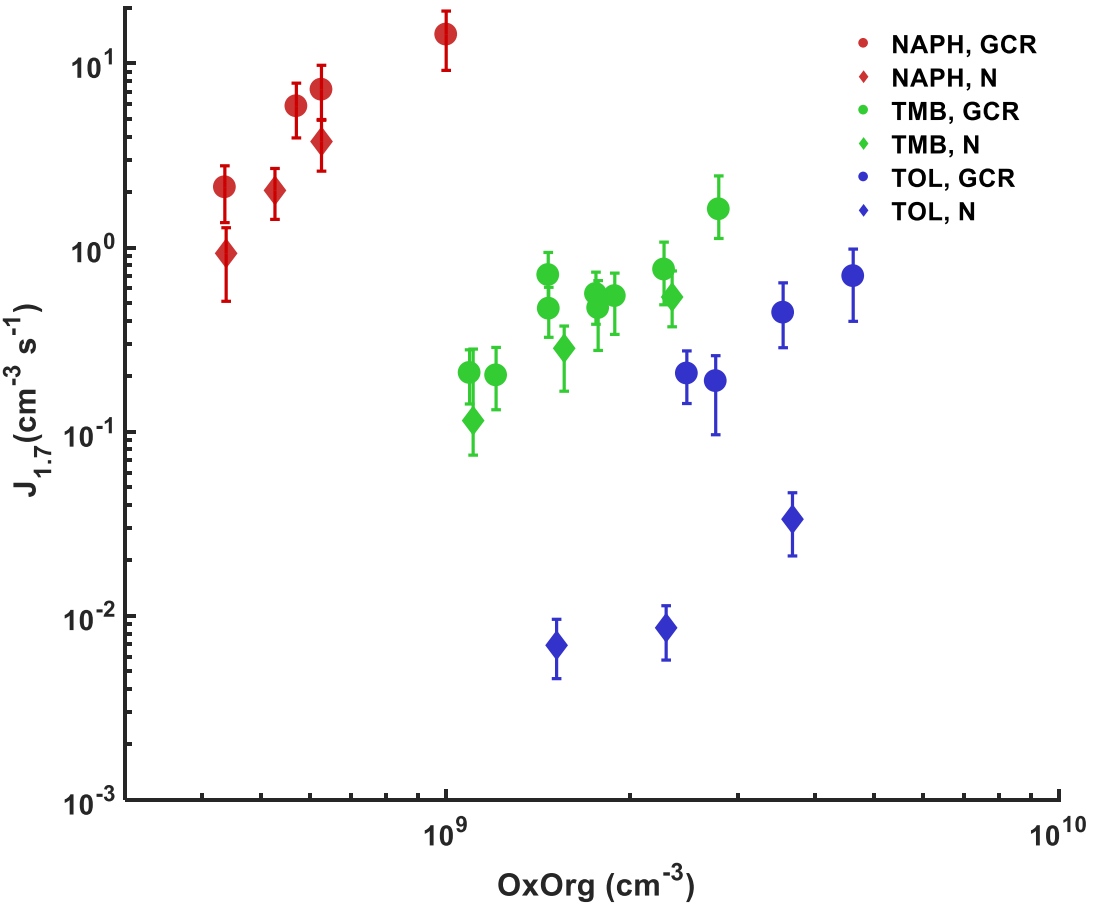

Figure S2: Dependence of particle formation rates from sulfuric acid and AVOC on OxOrg concentration at 293K. Experiments were conducted at 293 K with no addition of NO_x or NH_3. H_2SO_4 concentration varied from 1×10^6 to 4×10^7 cm^{-3} in these experiments, but had no effect on the nucleation rate in the absence of ammonia (Lehtipalo et al., 2018). Concentration of precursors in the experiments: 2-8 ppbv naphthalene (NAPH), 4 ppbv 1,2,4-trimethylbenzene (TMB), 40 ppbv toluene (TOL). Experiments under both neutral (N) and GCR conditions are shown. The *J* values for NAPH are even higher than for pure biogenic nucleation from BVOC (Kirkby et al., 2016) for the same amount of VOC reacted. However, these values are not relevant for the ambient atmosphere, in contrast to the BVOC, as AVOC are typically emitted together with NOx.

A

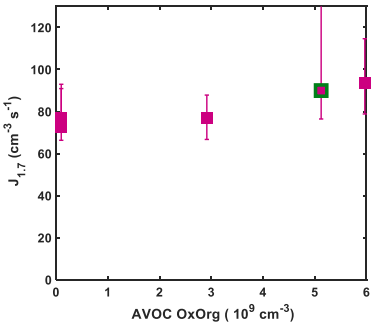

B

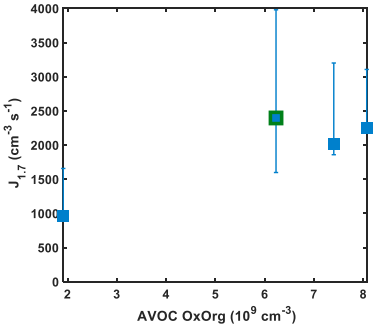

Figure S3. Dependence of particle formation rates from sulfuric acid, ammonia, DMA, and AVOC on OxOrg concentration at (A) 293 K and (B) 278 K. (A) Experiments with 7.4±0.4 ×10^6 cm^{-3} H_2SO_4, 800 to 2000 pptv NH_3, 4 pptv DMA and 0.71±0.18 ppbv NO at 293 K, with NAPH:TMB:TOL of 1:5:15. Symbol highlighted with green outline also has 1 ppbv α-pinene added to the experiment. Error bars present variation of the measurements. **(B)** Experiments with 5.1±0.6 ×10^6 cm^{-3} H_2SO_4, 1000 to 1500 pptv NH_3, 4 pptv DMA and 0.67±0.4 ppbv NO at 293 K, with NAPH:TMB:TOL of 1:5:20. Symbol highlighted with green outline also has 1 ppbv α-pinene added to the experiment. Error bars present variation of the measurements.

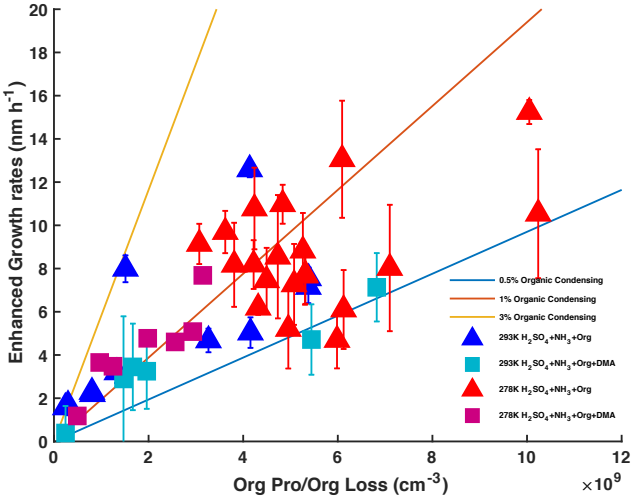

Figure S4. Enhanced growth rates of sub-3 nm particles by OxOrg. CLOUD data recorded at 278 K (blue and cyan) or 293 K (red and magenta) with 1×10^6 to 1×10^8 cm^{-3} H_2SO_4 and 1 to 2 ppbv NH_3 at GCR conditions. Experiments without DMA are shown by triangles, and with 4 pptv DMA by squares. Enhanced growth rates are calculated as measured growth rates minus the growth rates resulting from condensing sulfuric acid alone. Solid lines display the percentage contribution of 0.5, 1, and 3% of OxOrg to the growth rate. No NOx dependence can be identified. The variability in condensable OxOrg yields is driven by NO_X concentrations, multi-generation chemistry and precursor composition, e.g., naphthalene oxidation leads to lower volatility products than the single-ring aromatics.

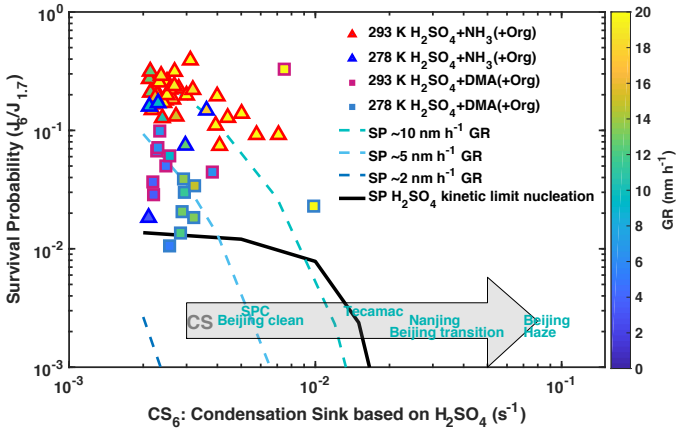

Figure S5. Survival probability (SP_6) of 6 nm particle vs condensation sink. Survival probability of 6 nm particles (SP_6) is calculated as the ratio between the nucleation rates at 1.7 and 6 nm. CLOUD data were recorded at 60% RH and 278 K (blue and cyan contours) or 293 K (red and magenta contours) with 1 to 2 ppbv NH_3. Experiments without DMA injection are shown by triangles and experiments with 4 pptv DMA by squares. The sub-3 nm growth rate is given by the colour of the symbols. The loss rates of newly formed particles are approximated by the condensation sink of sulfuric acid to particles larger than 6 nm (x-axis). Dashed lines are calculated survival probabilities of 6 nm particles with growth rates of 2, 5, and 10 nm h^{-1}. The solid line is the survival probability of 6 nm particles if 8 x 10^6 cm^{-3} sulfuric acid nucleates at the kinetic limit, which corresponds to a nucleation rate $J_{1.7}$ of 4000 cm^{-3} s^{-1} (Fig. 1a) and a sub-3 nm growth rate of 11 nm h^{-1} (Fig. 4A) under CLOUD chamber wall loss conditions. The high production rate of nucleating clusters significantly reduces the survival

probability and simultaneously increases the growth rate, and the survival probability only becomes dependent on CS once the latter is greater than the loss due to cluster-cluster collisions.

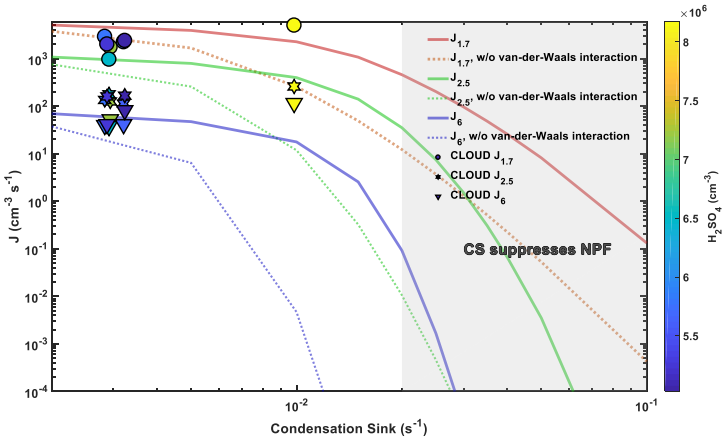

Figure S6. Dependence of particle formation rates at different diameters on condensation sink. Solid lines are simulated formation rates at different particle sizes for 10^7 cm^{-3} sulfuric acid nucleating at the kinetic limit considering van-der-Waals interaction. Dashed lines present the formation rates if van-der-Waals interaction is ignored and only hard sphere collisions are considered. CLOUD measurements are shown for 278 K in the presence of DMA. Grey shading denotes the area where NPF is suppressed for our range of conditions.

Table S1. Experimental conditions of data in Figure 1.

Run	$J_{1.7}$ (cm^{-3} s^{-1})	SA (cm^{-3})	NH_3 (ppb)	DMA (ppt)	NPT (ppb)	TMB (ppb)	TOL (ppb)	NO (ppb)	Temperature
1833.04	17	5.89E+07	1.4	N/A	N/A	N/A	N/A	N/A	293 K
1833.06	29	7.76E+07	1.4	N/A	N/A	N/A	N/A	N/A	293 K
1833.1	4.5	2.59E+07	1.4	N/A	N/A	N/A	N/A	N/A	293 K
1833.12	18	6.04E+07	1.4	N/A	N/A	N/A	N/A	N/A	293 K
1833.17	26	7.04E+07	1.4	N/A	N/A	N/A	N/A	N/A	293 K
1833.23	0.2	7.48E+06	1.4	N/A	N/A	N/A	N/A	N/A	293 K
1843.02	2.4	1.02E+07	0.8	N/A	3.3	6.9	39	0.21	293 K
1843.04	7.9	1.24E+07	0.8	N/A	3.3	6.2	39	0.16	293 K
1843.06	9.3	1.19E+07	0.8	N/A	3.3	6.2	39	0.15	293 K
1843.09	12	1.18E+07	0.8	N/A	3.3	6.2	39	0.15	293 K
1844.01	8.4	2.16E+07	1	N/A	3.9	7.6	40	0.29	293 K
1844.02	24	2.44E+07	0.8	N/A	3.7	6.7	39	0.2	293 K
1844.04	26	2.88E+07	0.9	N/A	3.6	6.6	39	0.21	293 K
1844.05	19	2.16E+07	0.8	N/A	3.3	6.1	39	0.16	293 K
1845.02	2.1	1.87E+07	1	N/A	3.8	7.7	40	1.4	293 K
1845.03	11	3.02E+07	0.8	N/A	3.4	6.8	39	1.2	293 K
1845.04	18	3.16E+07	0.8	N/A	3.3	6	39	0.98	293 K
1845.06	24	3.31E+07	0.8	N/A	3.3	5.7	39	0.91	293 K
1845.07	18	3.16E+07	0.8	N/A	3.1	5.3	38	0.79	293 K
1846.05	8	2.44E+07	0.9	N/A	3.6	6.8	39	0.64	293 K
1846.09	17	3.16E+07	0.8	N/A	3.4	5.5	38	0.49	293 K
1846.15	35	2.88E+07	0.8	N/A	3.2	4.9	38	0.41	293 K
1847.01	2.3	1.73E+07	1	N/A	3.8	7.8	40	1.2	293 K
1847.02	9.7	2.59E+07	0.9	N/A	3.7	6.9	39	1.2	293 K
1847.03	10	2.73E+07	0.8	N/A	3.5	6.4	39	1.1	293 K
1847.05	14	2.59E+07	0.8	N/A	3.4	6.1	39	1.1	293 K
1847.07	26	3.02E+07	0.8	N/A	3.5	6	39	1	293 K
1847.12	4.6	2.16E+07	1	N/A	3.9	7.7	12	0.63	293 K
1847.13	18	3.02E+07	0.9	N/A	3.5	6.2	11	0.59	293 K
1847.14	29	2.88E+07	0.8	N/A	3.5	5.5	10	0.52	293 K

1847.15	39	2.73E+07	0.8	N/A	3.7	5.4	9.6	0.47	293 K
1848.01	6.1	2.30E+07	1.1	N/A	1.6	7.7	39	0.61	293 K
1848.02	18	3.31E+07	0.9	N/A	1.6	6.4	39	0.54	293 K
1848.04	34	3.45E+07	0.9	N/A	1.7	5.9	38	0.46	293 K
1848.06	81	3.74E+07	0.9	N/A	1.8	5.8	38	0.44	293 K
1849.01	12	2.88E+07	1.3	N/A	4.4	1.6	40	0.6	293 K
1849.02	30	3.31E+07	1.3	N/A	3.6	1.2	39	0.55	293 K
1849.03	34	2.88E+07	1.2	N/A	3.2	1.1	38	0.48	293 K
1849.05	130	3.02E+07	1.2	N/A	3.3	1.1	38	0.46	293 K
1969.18	1.1	7.80E+06	0.6	N/A	0.54	2.7	12	0.06	293 K
1969.2	2.3	9.20E+06	0.6	N/A	0.48	2.6	12	0.06	293 K
1970.02	2.7	9.60E+06	0.8	N/A	0.51	2.4	12	0.03	293 K
1970.03	1.8	8.90E+06	0.9	N/A	0.49	2.3	12	0.04	293 K
1970.06	3.8	1.10E+07	1	N/A	0.47	2.2	12	0.04	293 K
1970.09	3.7	1.20E+07	0.6	N/A	0.44	1.9	11	0.05	293 K
1970.12	2.2	1.10E+07	0.8	N/A	0.44	2.2	11	0.07	293 K
1971.02	1	9.40E+06	0.6	N/A	0.49	4.2	12	0.44	293 K
1971.05	1	1.10E+07	0.5	N/A	0.44	2.3	11	0.46	293 K
1971.08	1.7	1.30E+07	0.6	N/A	0.41	2.2	11	0.68	293 K
1971.11	1.6	1.20E+07	0.6	N/A	0.42	2.3	11	0.65	293 K
1971.22	16	5.00E+07	0.7	N/A	0.42	1.5	11	0.56	293 K
1971.25	10	3.00E+07	0.5	N/A	1.5	9.1	45	0.26	293 K
1974.07	19	5.60E+06	0.9	3.1	N/A	N/A	N/A	0.17	293 K
1974.12	1.6	2.70E+06	1	2.6	N/A	N/A	N/A	0.06	293 K
1974.14	72	7.10E+06	0.8	2.8	N/A	N/A	N/A	0.37	293 K
1974.16	77	7.10E+06	0.7	3.1	N/A	N/A	N/A	0.62	293 K
1974.19	0.3	1.10E+06	0.8	3	N/A	N/A	N/A	0.05	293 K
1975.02	5.2	3.10E+06	1.1	4.2	0.1	0.68	2.3	0.12	293 K
1975.03	94	7.50E+06	1.1	3.8	0.1	0.53	2.1	0.58	293 K
1975.05	4.1	2.90E+06	0.7	3.8	0.28	0.75	2.1	0.16	293 K
1975.06	98	6.90E+06	0.8	3.8	0.23	0.52	2	0.82	293 K
1975.08	2.1	2.40E+06	0.8	3.7	0.33	1.5	3.9	0.2	293 K
1975.09	77	6.50E+06	0.7	3.5	0.23	1.1	3.4	0.89	293 K

1975.11	2.7	2.60E+06	0.6	3.7	0.56	3.1	7.8	0.17	293 K
1975.12	94	7.00E+06	0.5	3.6	0.41	2.3	6.7	0.69	293 K
1975.14	90	7.20E+06	0.4	3.4	0.06	2.2	6.7	0.81	293 K
1975.21	180	7.80E+06	0.6	3.8	0.43	2.7	9.5	0.8	293 K
1972.07	17	4.40E+06	1.1	N/A	0.55	2.6	15	0.24	278 K
1972.1	37	6.50E+06	0.9	N/A	0.45	2.2	15	0.34	278 K
1972.13	50	8.30E+06	0.6	N/A	0.35	1.8	15	0.58	278 K
1972.18	43	7.00E+06	0.7	N/A	0.44	2.2	15	0.44	278 K
1972.21	7.8	4.90E+06	0.6	N/A	0.11	0.64	3.9	0.08	278 K
1973.03	21	8.20E+06	0.6	N/A	0.06	0.25	3.5	0.68	278 K
1973.06	18	8.30E+06	0.8	N/A	0.01	0.13	1	0.78	278 K
1973.1	190	1.60E+07	0.6	N/A	0.26	1.8	13	1.3	278 K
1976.02	21	9.90E+05	0.8	4.2	N/A	N/A	N/A	1.6	278 K
1976.04	1.7	6.30E+05	0.6	5.4	N/A	N/A	N/A	0.14	278 K
1976.05	27	1.10E+06	0.6	5.3	N/A	N/A	N/A	0.13	278 K
1976.07	160	2.00E+06	0.6	4.6	N/A	N/A	N/A	0.34	278 K
1976.09	300	2.70E+06	0.5	4.6	N/A	N/A	N/A	0.88	278 K
1976.11	470	3.60E+06	0.4	3.9	N/A	N/A	N/A	1.9	278 K
1976.13	1700	6.70E+06	0.7	3.8	N/A	N/A	N/A	1.6	278 K
1977.01	690	4.20E+06	0.7	4.8	DL	0.63	2.7	0.3	278 K
1977.05	970	6.00E+06	0.8	3.8	DL	0.48	2.5	1.1	278 K
1977.07	310	2.80E+06	0.7	5	0.19	0.61	2.7	0.24	278 K
1977.09	2900	5.40E+06	0.6	5	0.12	0.48	2.6	0.93	278 K
1977.11	370	2.80E+06	0.5	5.5	0.23	1.2	4.5	0.25	278 K
1977.13	2200	5.30E+06	0.5	5.2	0.2	0.96	4.4	0.94	278 K
1977.15	340	2.70E+06	0.6	6.1	0.46	2.7	8.8	0.23	278 K
1977.17	2000	4.90E+06	0.6	6.1	0.42	2.2	8.6	0.68	278 K
1977.19	2400	4.70E+06	0.7	5.2	0.41	2.1	8.7	0.66	278 K
1977.2	5000	7.60E+06	0.7	4.7	0.29	1.3	8	0.46	278 K
1977.22	910	4.50E+06	0.7	4.5	0.3	1.6	8.1	0.64	278 K

N/A: not added.

DL: detection limit.

Table S2. nucleation rates, growth rates, condensation sinks, temperature, and precursors of NPF.

	J (cm^{-3} s^{-1})	GR (nm h^{-1})	H_2SO_4 (cm^{-3})	NH_3	Amine	Org (cm^{-3})	season	Temp (℃)	CS (s^{-1})
Tecamac[a]	162 (17~2057)	20 (7.8~>39)	7×10^6-1.7×10^7-6.6×10^7				end of March to early April	10-29	0.01-0.035
Beijing, Spring[b]	46.4 (17.7-156)	2.4 (1.2-3.3)	2×10^5-1.6×10^6	10 ppb[d]			March	8-24	0.0028 (clean), 0.02 (transition), 0.07 (haze)
Beijing, Winter[c]	26(12-38)	3.5 (0.5-9)					end of October to January	-15-20	0.0042 (0.0023-0.0057)
Beijing[e]	3-100		3×10^6-1×10^7		5-32 ppt		All year round		0.017
Nanjing, warm[f]	92-300	1.6-7.1	1.3×10^7-3.1×10^7			1.7×10^7-8.5×10^7			0.016-0.019
Nanjing, cold[f]	190-2500	4.2-8.8	3.5×10^7-4.8×10^7			1.1×10^8-1.7×10^8			0.028-0.033
YRD[g]	80	12.5					winter		0.026±0.014
SPC[h]	45 (23-53)	4.3 (1-10)						20-35	0.005-0.025
Madrid[i]	1.1-6.7	2.4-15.7					summer		3.40E-03
MAJ[i]	0.7-6.8	1.9-8.1							2.50E-03
Shanghai[j]	105 (42-207)	1.4 (0.55-3.3)	4×10^6-2×10^7		~100 pptv		All year round		~0.02
CLOUD H_2SO_4+DMA 278 K[h]	160-2475	1.72-18	6.3×10^5-7.6×10^6	1-2.5 ppb	4 pptv	HOMs up to 5×10^7 OxOrg up to 8.8×10^9		5	0.002-0.01

CLOUD H_2SO_4+DMA 293 K[h]	2.4-231	1.6-6.8	1×10^6-7.8×10^6	1-2.5 ppb	4 pptv	HOMs up to 8×10^7 OxOrg up to 6×10^9		20	0.002-0.008
CLOUD H_2SO_4+NH_3 278 K[h]	15-537	3.2-17.4	5×10^6-1.5×10^7	1-2.5 ppb	Not added	HOMs up to 3×10^7 OxOrg up to 9.6×10^9		5	0.002-0.004
CLOUD H_2SO_4+NH_3 278 K[h]	0.17-27	2.4-22	7.4×10^6-7.9×10^7	1-2.5 ppb	Not added	HOMs up to 3×10^8 OxOrg up to 9.2×10^9		20	0.002-0.007

[a](Kuang et al., 2008), [b](Cai et al., 2017), [c](Jayaratne et al., 2017), [d](Guo et al., 2017), [e](Cai et al., 2021), [f](Yu et al., 2016), [g](Dai et al., 2017), [h](Kontkanen et al., 2016), [h](Carnerero et al., 2018), [j](Yao et al., 2018), [h]this study.

90

Reference:

Berndt, T., Scholz, W., Mentler, B., Fischer, L., Herrmann, H., Kulmala, M. and Hansel, A.: Accretion product formation from self- and cross-reactions of RO 2 radicals in the atmosphere, Angew. Chemie Int. Ed., 57(14), 3820–3824, doi:10.1002/anie.201710989, 2018.

Cai, R., Yang, D., Fu, Y., Wang, X., Li, X., Ma, Y., Hao, J., Zheng, J. and Jiang, J.: Aerosol surface area concentration: a governing factor in new particle formation in Beijing, Atmos. Chem. Phys., 17(20), 12327–12340, doi:10.5194/acp-17-12327-2017, 2017.

Cai, R., Yan, C., Yang, D., Yin, R., Lu, Y., Deng, C., Fu, Y., Ruan, J., Li, X., Kontkanen, J., Zhang, Q., Kangasluoma, J., Ma, Y., Hao, J., Worsnop, D. R., Bianchi, F., Paasonen, P., Kerminen, V., Liu, Y., Wang, L., Zheng, J., Kulmala, M. and Jiang, J.: Sulfuric acid–amine nucleation in urban Beijing, Atmos. Chem. Phys., 21(4), 2457–2468, doi:10.5194/acp-21-2457-2021, 2021.

Carnerero, C., Pérez, N., Reche, C., Ealo, M., Titos, G., Lee, H. K., Eun, H. R., Park, Y. H., Dada, L., Paasonen, P., Kerminen, V. M., Mantilla, E., Escudero, M., Gómez-Moreno, F. J., Alonso-Blanco, E., Coz, E., Saiz-Lopez, A., Temime-Roussel, B., Marchand, N., Beddows, D. C. S., Harrison, R. M., Petäjä, T., Kulmala, M., Ahn, K. H., Alastuey, A. and Querol, X.: Vertical and horizontal distribution of regional new particle formation events in Madrid, Atmos. Chem. Phys., 18(22), 16601–16618, doi:10.5194/acp-18-16601-2018, 2018.

Dai, L., Wang, H., Zhou, L., An, J., Tang, L., Lu, C., Yan, W., Liu, R., Kong, S., Chen, M., Lee, S. and Yu, H.: Regional and local new particle formation events observed in the Yangtze River Delta region, China, J. Geophys. Res., 122(4), 2389–2402, doi:10.1002/2016JD026030, 2017.

Guo, H., Weber, R. J. and Nenes, A.: High levels of ammonia do not raise fine particle pH sufficiently to yield nitrogen oxide-dominated sulfate production, Sci. Rep., 7(1), 12109, doi:10.1038/s41598-017-11704-0, 2017.

Hanson, D. R., Bier, I., Panta, B., Jen, C. N. and McMurry, P. H.: Computational fluid dynamics studies of a flow reactor: free energies of clusters of sulfuric acid with NH3 or dimethyl amine, J. Phys. Chem. A, 121(20), 3976–3990, doi:10.1021/acs.jpca.7b00252, 2017.

Jayaratne, R., Pushpawela, B., He, C., Li, H., Gao, J., Chai, F. and Morawska, L.: Observations of particles at their formation sizes in Beijing, China, Atmos. Chem. Phys., 17, 8825–8835, doi:10.5194/acp-17-8825-2017, 2017.

Kirkby, J., Duplissy, J., Sengupta, K., Frege, C., Gordon, H., Williamson, C., Heinritzi, M., Simon, M., Yan, C., Almeida, J., Tröstl, J., Nieminen, T., Ortega, I. K., Wagner, R., Adamov, A., Amorim, A., Bernhammer, A.-K., Bianchi, F., Breitenlechner, M., Brilke, S., Chen, X., Craven, J., Dias, A., Ehrhart, S., Flagan, R. C., Franchin, A., Fuchs, C., Guida, R., Hakala, J., Hoyle, C. R., Jokinen, T., Junninen, H., Kangasluoma, J., Kim, J., Krapf, M., Kürten, A., Laaksonen, A., Lehtipalo, K., Makhmutov, V., Mathot, S., Molteni, U., Onnela, A., Peräkylä, O., Piel, F., Petäjä, T., Praplan, A. P., Pringle, K., Rap, A., Richards, N. A. D., Riipinen, I., Rissanen, M. P., Rondo, L., Sarnela, N., Schobesberger, S., Scott, C. E., Seinfeld, J. H., Sipilä, M., Steiner, G., Stozhkov, Y., Stratmann, F., Tomé, A., Virtanen, A., Vogel, A. L., Wagner, A. C., Wagner, P. E., Weingartner, E., Wimmer, D., Winkler, P. M., Ye, P., Zhang, X., Hansel, A., Dommen, J., Donahue, N. M., Worsnop, D. R., Baltensperger, U.,

Kulmala, M., Carslaw, K. S. and Curtius, J.: Ion-induced nucleation of pure biogenic particles, Nature, 533(7604), 521–526, doi:10.1038/nature17953, 2016.

Kontkanen, J., Järvinen, E., E. Manninen, H., Lehtipalo, K., Kangasluoma, J., Decesari, S., Paolo Gobbi, G., Laaksonen, A., Petäjä, T. and Kulmala, M.: High concentrations of sub-3nm clusters and frequent new particle formation observed in the Po Valley, Italy, during the PEGASOS 2012 campaign, Atmos. Chem. Phys., 16(4), 1919–1935, doi:10.5194/acp-16-1919-2016, 2016.

Kuang, C., McMurry, P. H., McCormick, A. V. and Eisele, F. L.: Dependence of nucleation rates on sulfuric acid vapor concentration in diverse atmospheric locations, J. Geophys. Res., 113(D10), D10209, doi:10.1029/2007JD009253, 2008.

Lehtipalo, K., Yan, C., Dada, L., Bianchi, F., Xiao, M., Wagner, R., Stolzenburg, D., Ahonen, L. R., Amorim, A., Baccarini, A., Bauer, P. S., Baumgartner, B., Bergen, A., Bernhammer, A. K., Breitenlechner, M., Brilke, S., Buchholz, A., Mazon, S. B., Chen, D., Chen, X., Dias, A., Dommen, J., Draper, D. C., Duplissy, J., Ehn, M., Finkenzeller, H., Fischer, L., Frege, C., Fuchs, C., Garmash, O., Gordon, H., Hakala, J., He, X., Heikkinen, L., Heinritzi, M., Helm, J. C., Hofbauer, V., Hoyle, C. R., Jokinen, T., Kangasluoma, J., Kerminen, V. M., Kim, C., Kirkby, J., Kontkanen, J., Kürten, A., Lawler, M. J., Mai, H., Mathot, S., Mauldin, R. L., Molteni, U., Nichman, L., Nie, W., Nieminen, T., Ojdanic, A., Onnela, A., Passananti, M., Petäjä, T., Piel, F., Pospisilova, V., Quéléver, L. L. J., Rissanen, M. P., Rose, C., Sarnela, N., Schallhart, S., Schuchmann, S., Sengupta, K., Simon, M., Sipilä, M., Tauber, C., Tomé, A., Tröstl, J., Väisänen, O., Vogel, A. L., Volkamer, R., Wagner, A. C., Wang, M., Weitz, L., Wimmer, D., Ye, P., Ylisirniö, A., Zha, Q., Carslaw, K. S., Curtius, J., Donahue, N. M., Flagan, R. C., Hansel, A., Riipinen, I., Virtanen, A., Winkler, P. M., Baltensperger, U., Kulmala, M. and Worsnop, D. R.: Multicomponent new particle formation from sulfuric acid, ammonia, and biogenic vapors, Sci. Adv., 4(12), eaau5363, doi:10.1126/sciadv.aau5363, 2018.

Leverentz, H. R., Siepmann, J. I., Truhlar, D. G., Loukonen, V. and Vehkamäki, H.: Energetics of atmospherically implicated clusters made of sulfuric acid, ammonia, and dimethyl amine, J. Phys. Chem. A, doi:10.1021/jp402346u, 2013.

Myllys, N., Kubečka, J., Besel, V., Alfaouri, D., Olenius, T., Smith, J. N. and Passananti, M.: Role of base strength, cluster structure and charge in sulfuric-acid-driven particle formation, Atmos. Chem. Phys., 19(15), 9753–9768, doi:10.5194/acp-19-9753-2019, 2019.

Ortega, I. K., Kupiainen, O., Kurtén, T., Olenius, T., Wilkman, O., Mcgrath, M. J., Loukonen, V. and Vehkamäki, H.: From quantum chemical formation free energies to evaporation rates, Atmos. Chem. Phys., 12, 225–235, doi:10.5194/acp-12-225-2012, 2012.

Schervish, M. and Donahue, N. M.: Peroxy radical chemistry and the volatility basis set, Atmos. Chem. Phys., 20(2), 1183–1199, doi:10.5194/acp-20-1183-2020, 2020.

Yao, L., Garmash, O., Bianchi, F., Zheng, J., Yan, C., Kontkanen, J., Junninen, H., Mazon, S. B., Ehn, M., Paasonen, P., Sipilä, M., Wang, M., Wang, X., Xiao, S., Chen, H., Lu, Y., Zhang, B., Wang, D., Fu, Q., Geng, F., Li, L., Wang, H., Qiao, L., Yang, X., Chen, J., Kerminen, V. M., Petäjä, T., Worsnop, D. R., Kulmala, M. and Wang, L.: Atmospheric new particle formation from sulfuric acid and amines in a Chinese megacity, Science, 361(6399), 278–281, doi:10.1126/science.aao4839, 2018.

Yu, H., Zhou, L., Dai, L., Shen, W., Dai, W., Zheng, J., Ma, Y. and Chen, M.: Nucleation and growth of sub-3 nm particles in

the polluted urban atmosphere of a megacity in China, Atmos. Chem. Phys., 16, 2641–2657, doi:10.5194/acp-16-2641-2016, 2016.